NUMERICAL INVESTIGATION OF HEAT TRANSFER AT A RECTANGULAR CHANNEL WITH COMBINED EFFECT OF NANOFLUIDS AND SWIRLING JETS IN A VEHICLE RADIATOR

by

Mustafa KILIC** and Asli ABDULVAHITOGLU
Department of Mechanical Engineering, Adana Science and Technology University, Adana, Turkey

Original scientific paper
https://doi.org/10.2298/TSCI180816294K

The present study is focused on the numerical investigation of heat transfer from a heated surface by using swirling jets and nanofluids. Consequences of discrete Reynolds number, inlet configuration and types of nanofluids (pure water, Al_2O_3-H_2O, Cu-H_2O, and TiO_2-H_2O) were studied numerically on heat transfer and fluid-flow. As a base coolant Al_2O_3-H_2O nanofluid was chosen for all parameters. So, a numerical analysis was done by using a k-ω turbulent model of PHOENICS CFD code. It is determined that increasing Reynolds number from Re = 12000-21000 causes an increment of 51.3% on average Nusselt Number. Using 1-jet causes an increase of 91.6% and 29.8% on average Nusselt number according to the channel flow and 2-jet. Using Cu-H_2O nanofluid causes an increase of 3.6%, 7.6%, and 8.5% on the average Nusselt number with respect to TiO_2-H_2O, Al_2O_3-H_2O and pure water.

Key words: *CFD, heat transfer, nanofluid, swirling jets*

Introduction

The cooling of a vehicle's engine is very important in terms of continuity of the performance of the vehicle. There is a lot of heat generation during engine operation and the radiator is used to removing this heat. In the existing cooling systems, the heat is removed by both conduction and convection. However, the heat transfer performance of the cooling fluid already used in radiators in the cooling system is not sufficient enough. At this point, the nanofluids attracted the attention of researchers. With the use of nanoparticles, the surface area of the heat transfer of the coolant can be increased, so that the heat transfer performance of the coolant can be increased. It has recently become an extremely important observation that highlights the superior heat transfer performance of the nanofluids [1, 2].

A nanofluid is defined as a suspension of solid particles which have 1-100 nm size in a base fluid. In heat transfer applications using nanofluid, the particles suspended in the base fluid, expand the thermal capacity of the fluid. Interactions and collisions between particles cause to increase in turbulence and turbulence intensity of the transition surface. Turbulence intensity and large surface area enable more heat transfer. Nanoparticles carry 20% of their atoms at the surface that makes them ready to heat transfer. Another advantage of using nanofluids is the particle agitation cause micro-convection in the fluid due to its very small size and therefore increases the heat transfer in particular heat transfer from surfaces with high heat flux, as well

* Corresponding author, e-mail: mkilic@adanabtu.edu.tr

as industry, medicine and space research. But the main disadvantages of using nanofluid may be a pressure drop and particle deposition in pipes or ducts. So using nanofluids with swirling jets may be a key solution for these disadvantages.

One of the main problems with the design parameter for new technological devices is heat loads. Using swirling flow with nanofluids can be a key solution to solve this heat loads problem. So, swirling flows have gained an increasing interest in the last decade in fluid dynamics research, since in many technical applications swirl is an essential phenomenon. Swirling flows are generally used in the industry for separation, mixing and flame stabilization. The main characteristic of swirling flow is the combination of axial and tangential velocities. Swirling flows are used to minimize pressure drop and prevent particle deposition, Kharoua *et al.* [3]. In swirling flows, part of the fluid enters axially while the remainder is injected tangentially at various locations along the tube axis. The radial pressure gradient results in thinning of thermal boundary later with an accompanying improvement in heat transfer, Chang *et al.* [4].

Many studies on enhancing heat transfer technique as impinging jets or swirling jets with different coolant can be found in the literature. Kilic *et al.* [5, 6] surveyed the cooling of a flat plate with the support of the impinging fluid air jet for different Reynolds numbers and dimensionless channel heights. Teamah *et al.* [7] investigated heat transfer and flow structure formed by Al_2O_3 nanofluid to flat plate by experimentally and numerically with various Reynolds number and the different volume ratio of nanofluids. Sun *et al.* [8] researched the effect of a single impinging jet using Cu-water nanofluids as working fluid on heat transfer. Kilic *et al.* [9] investigated the heat transfer from high heat flux surfaces for different parameters using nanofluids and multiple impinging jets. It was found that the increase in Reynolds number and decrease in particle diameter causes an increase in heat transfer. Sekrani *et al.* [10] investigated turbulent convective heat transfer of Al_2O_3 nanofluid flowing in a circular tube with uniform heat flux for different turbulence model numerically. Wongcharee *et al.* [11] investigated effects of swirling impinging jets with TiO_2-water nanofluid on heat transfer for different jet-to-target spacing ratio, Reynolds number and volume concentration. Akyurek *et al.* [12] studied turbulent forced convection heat transfer and pressure drop characteristic of Al_2O_3-water nanofluid experimentally by using wire coil turbulators.

This study is different from the studies at literature by evaluating the combined effect of swirling jets and nanofluids on heat transfer for different parameters to prevent the disadvantages (pressure drop and particle deposition) of nanofluids. By using the combined effect of nanofluids and swirling flows heat transfer enhancement was evaluated for different Reynolds number, different types of nanofluid and different inlet configuration. Numerical results were also validated with the experimental results in the literature.

Numerical model

The computational domain consists of a rectangular channel of which dimensions are 10×10×50 mm. Two jet inlets of which dimensions are 3×3 mm were located at the inverse direction to inject tangentially. There is one outlet at the end of the channel. All walls have a constant wall temperature. Inlet velocity of swirling jets is applied according to the Reynolds number. Effect of using nanofluids on heat transfer is determined by comparing nanofluids results with pure water results. Three parameters are applied to the condition of 2-jet. For the evaluation of different inlet configuration, 2-jet flow was compared with channel flow, 1-jet flow and 4-jet flow. k-ω turbulence model of PHOENICS CFD code was used

for this numerical analysis. CFD simulation domain is shown in fig. 1. Mesh structure is shown in fig. 2.

The continuity, Reynolds averaged momentum and time-averaged energy equations governing 3-D steady, the flow of fluid with constant properties used for turbulent solutions can be written in the Cartesian co-ordinate system as follows, eqs. (1)-(3):

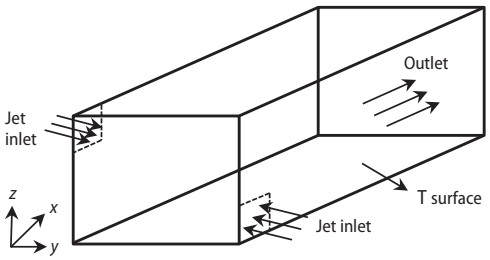

Figure 1. The CFD Simulation model

– continuity equation:

$$\frac{\partial U_i}{\partial x_i} = 0 \tag{1}$$

– momentum equation:

$$\rho U_i \frac{\partial U_j}{\partial x_i} = -\frac{\partial P}{\partial x_j} + \frac{\partial}{\partial x_i}\left[\mu\left(\frac{\partial U_i}{\partial x_j} + \frac{\partial U_j}{\partial x_i}\right) - \rho\overline{u_i' u_j'}\right] \tag{2}$$

– energy equation:

$$\rho c_p U_i \frac{\partial T}{\partial x_i} = \frac{\partial}{\partial x_i}\left[k\frac{\partial T}{\partial x_i} - \rho c_p \overline{u_i' T'}\right] \tag{3}$$

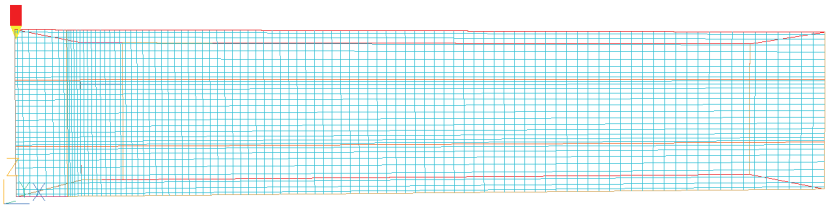

Figure 2. Mesh structure

Since Reynold number is higher than 10000. It was assumed that fluid is turbulent. So, a numerical analysis was done by using a k-ω turbulent model of PHOENICS CFD code. The k-ω turbulence model involves the solution of transport equations for the turbulent kinetic energy, k, and the turbulence frequency, ω. The ω can be defined as the specific dissipation rate ε/k where ε is the dissipation rate of k. In this study, a k-ω turbulence model is preferred since it performs better in transitional flows and internal flows with adverse pressure gradients. Additionally, the model is numerically very stable, it means this model can produce converged solutions more rapidly than the other models. All boundary conditions used in the study are summarized in tab 1. It was used 100×30×32 (96000 elements) meshes for this application. Mesh structure was prepared according to flow conditions. In order to get more precise numerical results, we intensified mesh numbers in some region as a jet inlet region and the surface of walls. Sweep number was studied between 2000 and 6000 and cell number was also studied between 24 and 36. It is observed that numerical geometry was independent of sweep number and cell number when sweep number was 3000 and cell number was 100×30×32. Variation of T_{avg} for different sweep number and grid number was shown in figs. 3 and 4.

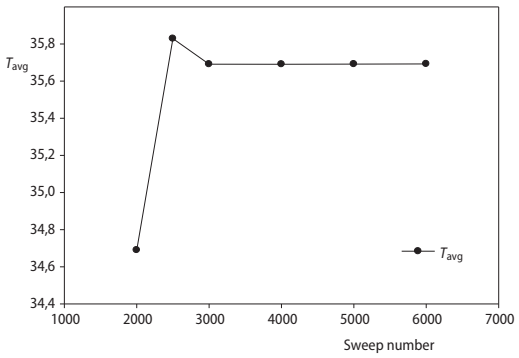

Figure 3. Variation of T_{avg} for different sweep number

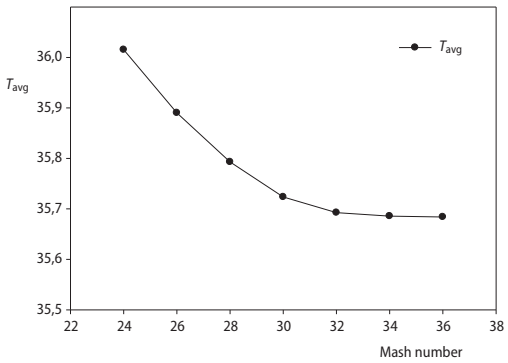

Figure 4. Variation of T_{avg} for different grid number

Table 1. Boundary conditions

	U [ms^{-1}]	V [ms^{-1}]	W [ms^{-1}]	T [°C]	k	ω
Inlet	$U = 0$	$V = V_{inlet}$	$W = 0$	$T = T_{inlet}$	K = (I.Inlet)	$\omega = \frac{\varepsilon}{Cd\,k}$
Outlet	$\frac{\partial U}{\partial x} = 0$	$\frac{\partial V}{\partial y} = 0$	$\frac{\partial W}{\partial z} = 0$	$T = T_{outlet}$	$\frac{\partial k}{\partial z} = 0$	$\frac{\partial \omega}{\partial z} = 0$
Bottom wall	$U = 0$	$V = 0$	$W = 0$	$T = T_{surface}$	$k = \frac{U\tau^2}{\sqrt{Cd}}$	$\omega = \frac{U\tau}{\sqrt{Cd}\,K\delta}$
Top wall	$U = 0$	$V = 0$	$W = 0$	$T = T_{surface}$	$k = \frac{U\tau^2}{\sqrt{Cd}}$	$\omega = \frac{U\tau}{\sqrt{Cd}\,K\delta}$
Front and back wall	$U = 0$	$V = 0$	$W = 0$	$T = T_{surface}$	$k = \frac{U\tau^2}{\sqrt{Cd}}$	$\omega = \frac{U\tau}{\sqrt{Cd}\,K\delta}$

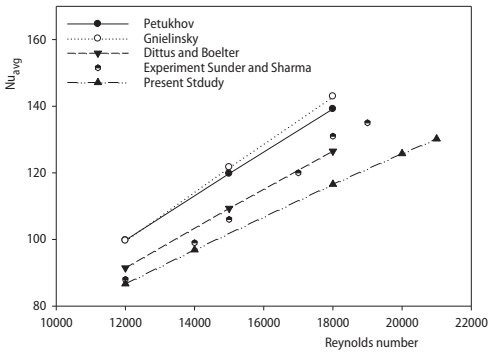

Figure 5. Verification of the model with experimental results and correlations

where $U\tau$ is the resultant friction velocity [$U\tau = (\tau_w/\rho)^{1/2}$], τ_w – the wall shear stress, δ – the normal distance of the first grid point from the wall, and k is von Karman's constant. Additionally, V_{inlet} – the bulk inlet velocity, I – the turbulent intensity (typically in the range $0.01 < I < 0.05$), ε – the dissipation rate ($\varepsilon = Cd^{3/4}k^{3/2}/L_m$), Cd – the constant ($Cd = 0.09$) and the mixing length $L_m \sim 0.1H$, where H is a characteristic inlet dimension. Numerical results were verified with the experimental results of Sunder and Sharma [13] and correlation of Petukhov, Gnielinsky, Dittus and Boelter, see in [10]. Verification of numerical model is shown in fig. 5. Difference between numerical results and experimental results is less than 11% for Re = 12000-18000.

Data reduction

The heat transfer from the surfaces to the fluid will take place by convection, conduction and radiation:

$$\dot{Q}_{\text{convection}} = \dot{Q}_{\text{total}} - \dot{Q}_{\text{conduction}} - \dot{Q}_{\text{radiaiton}} \tag{4}$$

Heat transfer occurs from high temperature walls to the nanofluid. So heat transfer rate gained by nanofluid equals the heat transfer rate lost by walls. As a result, walls surfaces will be cooled by using nanofluid with swirling jet. It is assumed that channel walls have a constant temperature. So heat conduction through the walls (from the outer surface to the inner surface) is neglected. Heat transfer with radiation is negligible in this study because the surface temperature is under 573.15 K.

Heat transfer rate gained by the fluid from wall surfaces:

$$\dot{Q} = \dot{m} C_{p\,(\text{nf})} (T_{\text{outlet}} - T_{\text{inlet}}) \tag{5}$$

where $\dot{m}$ is the mass-flow rate of nanofluid, $C_{p(\text{nf})}$ – the nanofluid specific heat, T_{outlet} – the outlet temperature of nanofluid, and T_{inlet} is the inlet temperature of nanofluid. Nusselt number is a dimensionless parameter indicating the ratio of heat transfer with convection to heat transfer with conduction. The average Nusselt number, eq. (6), can be presented as the ratio of the average heat transfer coefficient times characteristic length, D_h, to the coefficient of thermal conductivity of the nanofluid.

$$\text{Nu}_{\text{avg}} = \frac{h_{\text{avg}} D_h}{k_{\text{nf}}} \tag{6}$$

where h_{avg} is the average heat transfer coefficient, measured, D_h – the hydraulic diameter, and k_{nf} – the coefficient of thermal conductivity of the nanofluid. Average heat transfer coefficient can be presented:

$$h_{\text{avg}} = \frac{\dot{Q}}{A_s T_{lm}} \tag{7}$$

where A_s is the convection surface area and T_{lm} is the logarithmic mean temperature of nanofluid:

$$T_{lm} = \frac{\Delta T_e - \Delta T_i}{\ln\left(\dfrac{\Delta T_e}{\Delta T_i}\right)} \tag{8}$$

where ΔT_e is the temperature difference between surface temperature and nanofluid exit temperature ($\Delta T_e = (T_s - T_e)$ and ΔT_i is temperature differenace between surface temperature and nanafluid inlet temperature ($\Delta T_i = (T_s - T_i)$. Reynolds number is used to determine for forced convection whether the flow is laminar or turbulent. Reynolds number based on turbulent flow:

$$\text{Re} = \frac{\rho_{\text{nf}} V_{\text{jet}} D_h}{\mu_{\text{nf}}} \tag{9}$$

where ρ_{nf} is the nanofluid density, V_{jet} – the jet velocity, and μ_{nf} – the nanofluid dynamic viscosity.

The density of nanofluids is:

$$\rho_{\mathrm{nf}} = (1-\varphi)\rho_{\mathrm{bf}} + \varphi\rho_{\mathrm{p}} \tag{10}$$

where ρ_{bf} is the base fluid (water) density, φ – the volumetric ratio of the nanofluid, and ρ_{p} – the density of the solid particles in the nanofluid. The volumetric ratio of nanoparticles is:

$$\varphi = \frac{1}{\frac{1}{\omega}\left(\rho_{\mathrm{p}} - \rho_{\mathrm{bf}}\right)} \tag{11}$$

where ω is the density difference between the fluid and the main fluid (water). The nanofluid specific heat is calculated from:

$$C_{p_{\mathrm{nf}}} = \frac{\varphi(\rho C_p)_{\mathrm{p}} + (1-\varphi)(\rho C_p)_{\mathrm{f}}}{\rho_{\mathrm{nf}}} \tag{12}$$

where $C_{p(\mathrm{p})}$ is the specific heat of particle $C_{p(\mathrm{f})}$ – the specific heat of base fluid. The effective thermal conductivity of nanofluid is calculated according to Corcione [14]:

$$\frac{k_{\mathrm{eff}}}{k_{\mathrm{f}}} = 1 + 4.4\,\mathrm{Re}^{0.4}\,\mathrm{Pr}\left(\frac{T_{\mathrm{nf}}}{T_{\mathrm{fr}}}\right)^{10}\left(\frac{k_{\mathrm{p}}}{k_{\mathrm{f}}}\right)^{0.03}\varphi^{0.66} \tag{13}$$

where Re is the nanoparticle Reynolds number, Pr – the Prandtl number of the base liquid. k_p – the nanoparticle thermal conductivity, φ – the volume ratio of the suspended nanoparticles, T_{nf} [K] – the nanofluid temperature, and T_{fr} – the freezing point of the base liquid.

Nanoparticle Reynolds number is defined:

$$\mathrm{Re} = \frac{2\rho f k_{\mathrm{b}} T}{\pi\mu f^2 d_p} \tag{14}$$

The k_{b} is the Boltzmann's constant. The effective dynamic viscosity of nanofluids defined:

$$\mu_{\mathrm{nf}} = \mu_{\mathrm{bf}}(1 + 2.5\varphi + 4.698\varphi^2) \tag{15}$$

Results and discussions

In this section, numerical results were prepared for four parameters. Effects of Al_2O_3-water nanofluid with 20 nm particle diameter and volume ratio of $\varphi = 4\%$ on heat transfer for different Reynolds number (Re = 12000, 15000, 18000, 21000), different inlet configuration (channel flow, 1-jet, 2-jet, 4-jet) were obtained. Additionally, the effects of different nanofluids on heat transfer (Al_2O_3-water, Cu-water, TiO_2-water, and pure water) were also explained.

Effects of different Reynolds number on heat transfer

To understand the effect of fluid velocity on heat transfer, the Reynolds number was increased from Re = 12000 to 21000. Figures 6 and 7 show velocity vector and temperature contours of fluid-flow at the midpoint of the inlet of swirling jet, in the middle of channel and outlet of the channel at x-direction (x/D_h = 0.03, 8, 16) for Re = 12000 and 21000, respectively.

Thermal boundary region does not occur at the inlet of swirling jet because of the high turbulence intensity at the surfaces of the channel. Temperature increase can be seen only in the impinging region of swirling jet because fluid velocity decreases at this region.

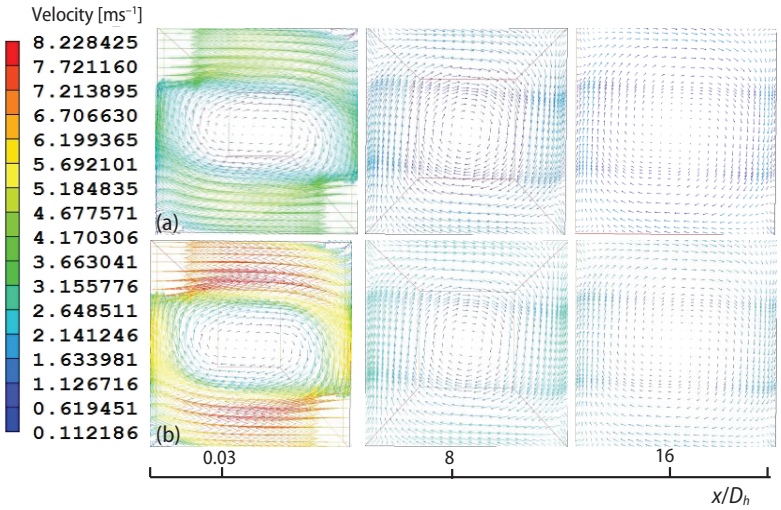

Figure 6. Velocity vectors for different Reynolds number; (a) Re = 12000 and (b) Re = 21000

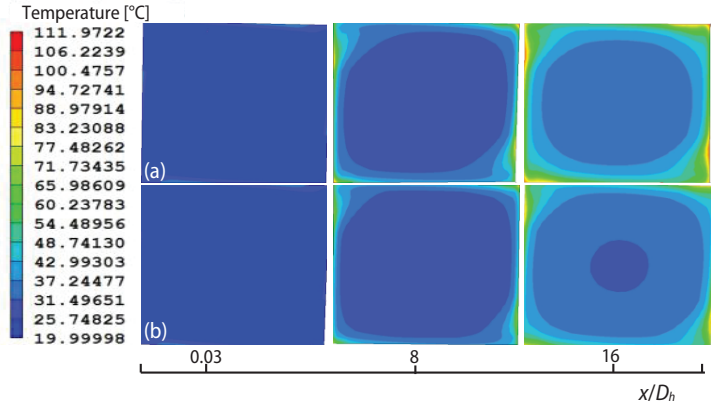

Figure 7. Temperature contours for different Reynolds number; (a) Re = 12000 and (b) Re = 21000

Velocity vector occurs in a shape of a flattened sphere. So the effect of swirling jet can be seen significantly at the inlet region of swirling jets. In the middle of the channel thermal boundary-layer is thickening because of the velocity decrease (decrease of the hydrodynamic boundary-layer) at the corner of the rectangular channel. This boundary-layer thickness increase can be seen at the direction of swirling flow. Since separation of fluid-flow is more evident in this region. At the end of the channel, a decrease of fluid velocity can be seen easily. Separation of the fluid-flow is more important at the corner of the channel at this region. Decreasing hydrodynamic boundary-layer thickness causes an increase in thermal boundary-layer thickness and it causes an increase in surface temperature. So increasing Reynolds number causes an increase in the hydrodynamic boundary-layer and a decrease of the thermal boundary-layer and surface temperature. Variation of average Nusselt number for different Reynolds number is shown in fig. 8.

It is obtained that increasing Reynolds number causes an increase in the average Nusselt number and decrease in surface temperature. So increasing the Reynolds number from 12000

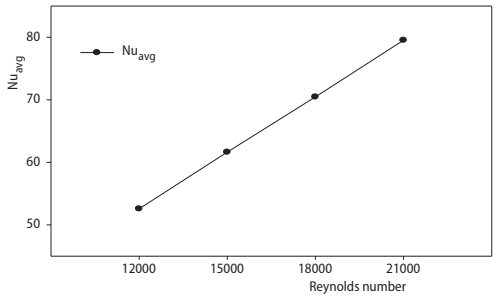

Figure 8. Average Nusselt number of Al_2O_3-H_2O nanofluid for different Reynolds number

to 21000 causes an increment of 51.3% on average Nusselt Number. But this increase decreases gradually. Increasing Reynolds number from Re = 12000 to 15000 causes an increment of 17.2% on the average Nusselt number. But the increase in Reynolds number from Re = 15000 to 18000 and Re = 18000 to 21000, the inclination decreases to 14.3% and 12.9%, respectively.

Effects of different types of nanofluid

Numerical analysis is conducted for a different type of nanofluid (Cu-H_2O, Al_2O_3-H_2O, TiO_2-H_2O, and H_2O) with 20 nm particle size and $\varphi = 4\%$ at Re = 18000 and $T_{inlet} = 20$ ºC. Properties of nanofluids were calculated at bulk film temperature. Table 2 shows thermophysical properties of nanofluids (density, specific heat, kinematic viscosity, thermal conductivity, and thermal expansion coefficient). Local Nuselt numbers show that nanofluids with higher thermal conductivity cause higher heat transfer rate and higher average Nusselt number.

Table 2. Thermophysical properties of nanofluids at 293 K

Nanofluid	Density, ρ [kgm^{-3}]	Specific heat, C_p [Jkg^{-1}K^{-1}]	Kinematic viscosity γ [m^{2}s^{-1}]	Thermal conductivity λ [Wm^{-1}K^{-1}]	Thermal expansion coefficient β
Cu-water	1157.43	3594.13	0.000000902	0.6422	0.0001544
TiO-water	1063.24	3902.51	0.000000982	0.6382	0.0001537
Al_2O_3-water	1055.84	3931.45	0.000000989	0.6378	0.0001534
Pure Water	998.20	4182.00	0.000000990	0.5970	0.0001430

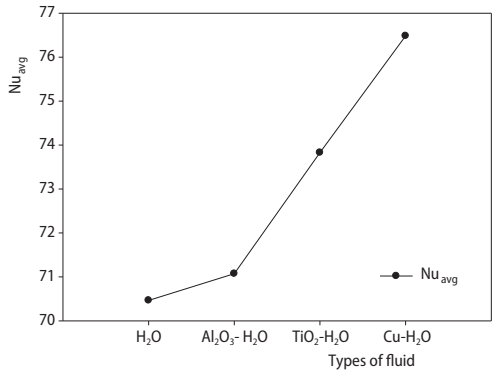

Figure 9. Average Nusselt numbers for the different type of nanofluids

Figure 9 shows variation in average Nusselt number for Cu-H_2O, Al_2O_3-H_2O, TiO-H_2O nanofluids, and H_2O. It was obtained that using Cu-H_2O nanofluid causes an increase of 3.6%, 7.6%, and 8.5% on the average Nusselt number with respect to TiO_2-H_2O, Al_2O_3-H_2O, and H_2O. It can be seen that using Cu-H_2O nanofluid shows better heat transfer performance.

Higher kinematic viscosity and higher thermal conductivity cause increasing heat transfer rate from the surface by increasing thermal boundary-layer thickness and decreasing hydrodynamic boundary-layer thickness. So increasing thermal conductivity or decreasing density and specific heat causes an increase in heat transfer rate. Temperature contours along the channel for different types of nanofluid are shown in fig. 10.

The current numerical study shows that using nanofluids in spite of traditional heat transfer fluids shows better heat transfer performance. Nanoparticles in the base fluid increase the thermal conductivity of the base fluid.

Effects of different inlet configuration

Four different inlet configurations are conducted to understand the effect of flow configuration on heat transfer for Al_2O_3-H_2O nanofluid. It is assumed that mass-flow rate is constant for all flow configurations. Velocity vectors and temperature contours at inlet and outlet region of the channel were shown in figs.11 and 12.

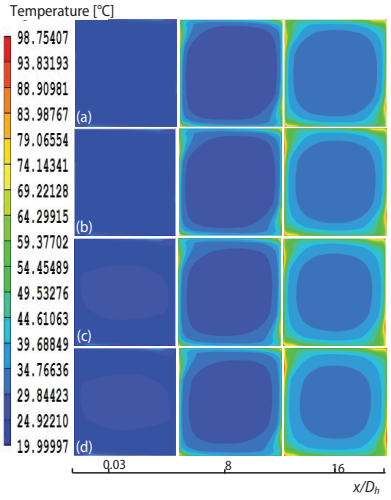

Figure 10. Temperature contours for different types of nanofluid; (a) H_2O (b) Al_2O_3-H_2O (c) TiO_2-H_2O, and (d) Cu-H_2O

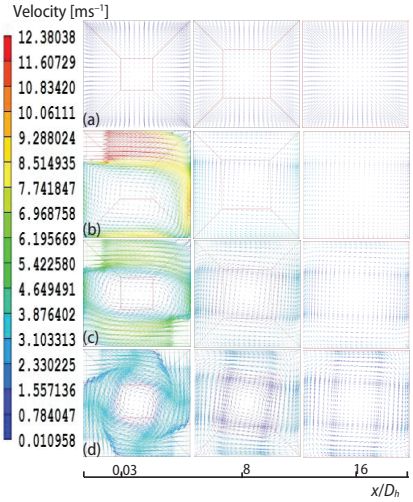

Figure 11. Velocity vectors for different inlet configuration; (a) channel flow (b) 1-jet flow (c) 2-jet flow (d) 4-jet flow

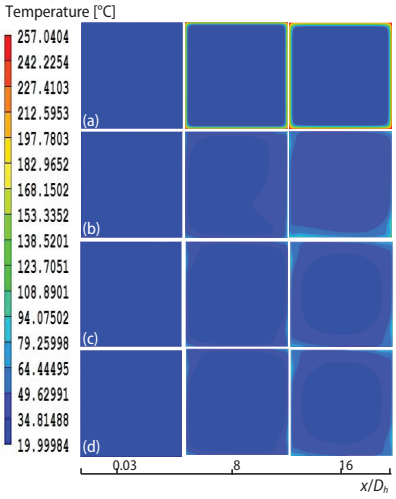

Figure 12. Temperature contours for different inlet configuration; (a) channel flow (b) 1-jet flow (c) 2-jet flow (d) 4-jet flow

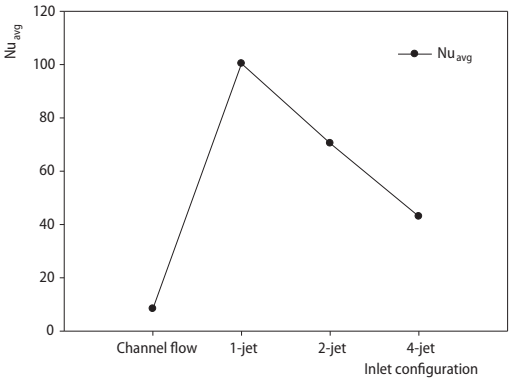

Figure 13. Average Nusselt number for different inlet configuration

It is obtained that 1-jet flow is compared with the 2-jet flow, 4-jet flow and channel flow. It is obtained that using 1-jet flow causes an increase of 91.6%, 29.8%, and 57.1% on the average Nusselt number with respect to channel flow, 2-jet flow and 4-jet flow. Average Nusselt numbers for different inlet configurations were shown in fig. 13.

Conclusions

The present study is focused on the numerical investigation of heat transfer from a heated surface by using nanofluids and swirling jets in a vehicle radiator. Effects of different Reynolds number, different inlet configuration and varies types of nanofluids (Al_2O_3-H_2O, Cu-H_2O, TiO_2-H_2O, and pure water) on heat transfer and fluid-flow were studied numerically. It is determined that increasing Reynolds number from Re = 12000 to 21000 causes an increment of 51.3% on average Nusselt number. Using 1-jet causes an increase of 91.6% and 29.8% on average Nusselt number according to the channel flow and 2-jet. Using Cu-H_2O nanofluid causes an increase of 3.6%, 7.6%, and 8.5% on the average Nusselt number with respect to TiO_2-H_2O, Al_2O_3-H_2O and pure water. Using Cu-H_2O nanofluids shows the best heat transfer performance. Difference between numerical results of this study and experimental results is less than 11% for Re = 12000-18000. Research areas for future investigations can be using different particle diameter, different volume ratio and different types of nanofluids with different application geometries and cooling techniques.

Acknowledgment

The financial support of this study by Scientific Research Projects (18103006 and 1610321) of Adana Science and Technology University is gratefully acknowledged.

Nomenclature

C_{pnf} – nanofluid specific heat, [Jkg^{-1}K^{-1}]
C_{pp} – particle specific heat, [Jkg^{-1}K^{-1}]
d_p – particle diameter, [nm]
k_{eff} – effective thermal conductivity, [Wm^{-1}K^{-1}]
k_{nf} – nanofluid thermal conductivity, [Wm^{-1}K^{-1}]
Nu_x – local Nusselt number, ($= QD_h\Delta T^{-1}k_{nf}^{-1}$), [–]
Nu_{avg} – average Nusselt number, ($= h_{avg}D_hk_{nf}^{-1}$), [–]

Greek Symbols

ρ_{bf} – base fluid density, [kgm^{-3}]
φ – nanoparticle volume ratio, [–]
μ_{nf} – dynamic viscosity of nanofluid, [kgm^{-1}s^{-1}]
μ_{bf} – base fluid dynamic viscosity, [kgm^{-1}s^{-1}]

References

[1] Jadar, R., *et al.*, Nanotechnology Integrated Automobile Radiator, *Mater. Today Proc., 4* (2017), 11, pp. 1280-1284
[2] Leong, K. Y., *et al.*, Performance Investigation of an Automotive Car Radiator Operated with Nanofluid-Based Coolants (Nanofluid as a Coolant in a Radiator), *Appl. Therm. Eng*., *30* (2010), 17-18, pp. 2685-2692
[3] Kharoua, N., *et al.*, The Interaction of Confined Swirling Flow with Conical Bluff Body: Numerical Simulation, *Chemical Engineering Research and Design*, *136* (2018), Aug., pp. 207-218
[4] Chang, F., Dhir, V. K., Turbulent Flow Field in Tangentially Injected Swirl Flows in Tubes, *Int. Jour. of Heat and Fluid Flow, 15* (1994), Oct., pp. 346-356
[5] Kilic, M., *et al.*, Experimental and Numerical Study of Heat Transfer from a Heated Flat Plate in a Rectangular Channel with an Impinging Jet, *Journal of the Brazilian Society of Mechanical Sciences and Engineering, 39* (2017), 1, pp. 329-344
[6] Kilic, M., Baskaya, S., Improvement of Heat Transfer from High Heat Flux Surfaces by Using Vortex Promoters with Different Geometries and Impinging Jets*, Journal of the Faculty of Engineering and Architecture of Gazi University, 32* (2017), 3, pp. 693-707

[7] Teamah, M. A., *et al.*, Numerical and Experimental Investigation of Flow Structure and Behavior of Nanofluids Flow Impingement on Horizontal Flat Plate, *Experimental Thermal and Fluid Science, 74* (2016), June, pp. 235-246
[8] Sun, B., *et al.*, Heat transfer of Single Impinging Jet with Cu Nanofluids, *Applied Thermal Engineering, 102* (2016), June, pp. 701-707
[9] Kilic, M., Ali, H. M., Numerical Investigation of Combined Effect of Nanofluids and Multiple Impinging Jets on Heat Transfer, *Thermal Science*, *23* (2018), 5B, pp. 3165-3173
[10] Sekrani, *et al.*, Modelling of Convective Turbulent Heat Transfer of Water-Based Al2O3 Nanofluids in an Uniformly Heated Pipe, *Chem. Eng. Sci., 176* (2018), Feb., pp.205-219
[11] Wongcharee, K., *et al.*, Heat Transfer of Swirling Impinging Jets with TiO2-Water Nanofluids, *Chem. Eng. and Porcessing*, *114* (2017), Apr., pp. 16-23
[12] Akyurek, E. F., *et al.*, Experimental Analysis of Nanofluid with Wire Coil Turbulators in a Concentric Tube Heat Exchanger, *Results in Physics*, *9* (2018), June, pp. 376-389
[13] Sundar, L. S., Sharma, K. V., Heat Transfer Enhancements of Low Volume Concentration Al2O3 Nanofluid and with Longitudinal Strip Inserts in a Circular Tube, *Int.J.of Heat and Mass Transfer, 53* (2010), 19-20, pp. 4280-4286
[14] Corcione, M., Empirical Correlating Equations for Predicting the Effective Thermal Conductivity and Dynamic Viscosity of Nanofluids, *Energy Conversation Management, 52* (2011), 1, pp. 789-93

Paper submitted: August 16, 2018
Paper revised: September 27, 2018
Paper accepted: October 1, 2018